materials

MDPI

Article

Improvement in NO_2 Gas Sensing Properties of Semiconductor-Type Sensors by Loading Pt into $BiVO_4$ Nanocomposites at Room Temperature

Wang-De Lin [1,*], Shu-Yun Lin [2] and Murthy Chavali [3,4]

[1] Department of Center for General Education, St. Mary's Junior College of Medicine, Nursing and Management, Yilan City 26647, Taiwan
[2] Department of Applied Chemistry, Providence University, Taichung City 43301, Taiwan; s1063051@gm.pu.edu.tw
[3] Office of the Dean (Research) & Division of Chemistry, Department of Sciences, Faculty of Sciences & Technology, Alliance University, Karnataka, Bengaluru 562106, India; siva.chavali@alliance.edu.in or ChavaliM@gmail.com
[4] NTRC-MCETRC and 109 Composite Technologies Pvt. Ltd., Andhra Pradesh, Guntur District, Guntur 522201, India
* Correspondence: newwander@smc.edu.tw

Abstract: In the present study, we report the first attempt to prepare a conducive environment for $Pt/BiVO_4$ nanocomposite material reusability for the promotion of sustainable development. Here, the $Pt/BiVO_4$ nanocomposite was prepared using a hydrothermal method with various weight percentages of platinum for use in NO_2 gas sensors. The surface morphologies and structure of the $Pt/BiVO_4$ nanocomposite were characterized by scanning electron microscope (SEM), transmission electron microscopy (TEM), energy-dispersive X-ray spectroscopy (EDX), and X-ray diffraction (XRD). The results showed that Pt added to $BiVO_4$ with 3 wt.% $Pt/BiVO_4$ was best at a concentration of 100 ppm NO_2, with a response at 167.7, and a response/recovery time of 12/35 s, respectively. The $Pt/BiVO_4$ nanocomposite-based gas sensor exhibits promising nitrogen dioxide gas-sensing characteristics, such as fast response, highly selective detection, and extremely short response/recovery time. Additionally, the mechanisms of gas sensing in $Pt/BiVO_4$ nanocomposites were explored in this paper.

Keywords: NO_2; gas sensors; $Pt/BiVO_4$; nanocomposite

Citation: Lin, W.-D.; Lin, S.-Y.; Chavali, M. Improvement in NO_2 Gas Sensing Properties of Semiconductor-Type Sensors by Loading Pt into $BiVO_4$ Nanocomposites at Room Temperature. *Materials* **2021**, *14*, 5913. https://doi.org/10.3390/ma14205913

Academic Editor: Gianfranco Dell'Agli

Received: 21 August 2021
Accepted: 4 October 2021
Published: 9 October 2021

1. Introduction

Nitrogen dioxide (NO_2) emissions are largely the result of fossil fuel combustion in automobiles and electrical power plants [1,2]. NO_2 exposure at concentrations as low as a few ppm can be dangerous to human health and higher concentrations have been linked to smog and acid rain [3,4]. In the current study, we developed a highly sensitive NO_2 sensor capable of detection at extremely low concentrations at room temperature [5–7]. One common approach to NO_2 detection involves nanostructures of bismuth vanadate ($BiVO_4$). Beyond NO_2 detection [8–10], $BiVO_4$ has been used in a wide variety of applications, such as formaldehyde degradation [11,12], H_2S production [13,14], hydrogen production [15,16], CO_2 capture [17,18], and other fields [19–21]. Table 1 lists a variety of NO_2 sensors based on Pt or $BiVO_4$. $BiVO_4$ is inexpensive, highly responsive to visible light, stable, non-toxic, and environmentally benign with a narrow bandgap of Eg = 2.4 eV [22]. However, the low charge transfer rate of $BiVO_4$ impedes efforts to enhance photocatalytic activity [23].

To improve charge transfer, various methods have been planned, including doping with various metals [24,25], the surface deposition of noble metals [26–28], and the formation of compound semiconductors [29,30]. The use of dopants has been shown to introduce

electronic barriers, which capture photogenerated electrons and transfer them to other materials to prevent electron-hole recombination.

In this study, we developed a novel Pt/$BiVO_4$ composite designed specifically for the sensing of NO_2 at room temperature.

Table 1. Comparison of the NO_2-sensing performance of different contents of Pt/$BiVO_4$ nanocomposites.

Sensing Material	Response Time (T_{90}, s)	Recovery Time (T_{r90}, s)	Response (100 ppm)	Pt Crystalline Size (by XRD) (nm), hkl, 111	Bi Crystalline Size $BiVO_4$ (by XRD) (nm), hkl		Linearity (R^2)
					(051)	(161)	
$BiVO_4$	72	44	91.3	-	24.8	26.5	0.983
0.5 wt.% Pt/$BiVO_4$	79	24	99.2	10.1	24.2	25.8	0.950
1 wt.% Pt/$BiVO_4$	64	51	143.5	10.6	25.2	27.7	0.982
3 wt.% Pt/$BiVO_4$	12	35	167.7	12.1	25.5	27.7	0.992
5 wt.% Pt/$BiVO_4$	95	102	173.9	12.9	25.8	28.2	0.980
10 wt.% Pt/$BiVO_4$	43	67	181.4	16.3	24.6	27.4	0.928

2. Materials and Methods

2.1. Materials

($Bi(NO_3)_3{\cdot}5H_2O$), (NH_4VO_3), ethanol (C_2H_5OH), nitric acid (HNO_3) ammonium hydroxide (NH_4OH), sodium borohydride ($NaBH_4$), ethylenediaminetetraacetic acid (EDTA), silver(I) nitrate ($AgNO_3$) and dihydrogen hexachloroplatinate (VI) hexahydrate ($H_2PtCl_6{\cdot}6H_2O$) were purchased from Sigma-Aldrich Co., Inc. (St. Louis, MO, USA). Distilled H_2O obtained using the distillation water system provided by the Millipore Corporation (Millipore Corp. Molsheim, France) was used.

2.2. Preparation of Bismuth Vanadate

Briefly, a few mmol of Bismuth nitrate (4 g) was added to 6.8 mmol of EDTA (2 g) in acidic medium (0.3 M), whereupon gradual heating to 85 °C was performed for the mixture to procure a colourless solution (named Solution A). A total of 8.5 mmol (1 g) of NH_4VO_3 was then dissolved in 50 mL of H_2O at 60 °C under vigorous stirring for the generation of a yellow solution (named Solution B). The above two solutions mentioned (i.e., Solution A + Solution B) were then further processed with mixing at 50 °C for 1 hour with controlled stirring, after which, the resulting mixture was controlled with pH adjustment to 3.0 by the addition of salt (1 M). The prepared mixed product was poured into the autoclave (Dogger, New Taipei City, Taiwan) made of stainless steel with Teflon lining and further covered with sealant, then kept for heating, which was maintained at 180 °C for 6 h. After cooling of the autoclave, the resultant product was withdrawn via centrifugation, before undergoing multiple washings using ultrapure water and ethanol, followed by drying in an oven at 80 °C overnight and calcination at 450 °C for 4 h to complete the synthesis of $BiVO_4$ [11].

2.3. Synthesis Method for Pt/$BiVO_4$ Nanocomposite

Distilled water containing a pre-calculated quantity of $H_2PtCl_6{\cdot}6H_2O$ was added to the as-prepared product of $BiVO_4$, which was dispersed in 100 mL and further maintained for 1 h at a continuous stirring rate. The precursor suspension was produced as the product was extracted for centrifugation, washed three times using DI water, and then three times again using alcohol. The precipitate obtained was prepared by drying at 80 °C for more than 6 h. Pt/$BiVO_4$ preparation was done with Pt at various weight concentrations labelled as follows: 0, 0.5, 1, 3, 5, or 10 wt.% Pt/$BiVO_4$.

2.4. Characterization

The proposed Pt/$BiVO_4$ nanocomposite was determined using a transmission electron microscope for morphology and structure with an energy-dispersive X-ray spectroscope (TEM/EDS; JEM-2100F), and a field emission scanning electron microscope (FESEM; JEOL JSM-7500F) operated at 30 kV. Pt/$BiVO_4$ was characterized to understand its crystal structure using a Shimadzu X-ray diffractometer at 1.5405 Å at 40 kV and 30 mA, supported by a vertical goniometer in the range of 10° to 80° (2theta) at a scan speed of 2°/min.

2.5. Sensor Fabrication and Measurements

The designed sensors were prepared by a dipping and coating procedure (Binder: PVA) on an alumina-based solid substrate (10 × 5 mm^2; and fab of chip-based sensor; rotational speed, 1000 rpm) in the prepared material, to fabricate an electrode with a comb-like structure. The chips were subsequently pretreated to 80 °C over a period of 0.5 h and then calcined at a temperature of 400 °C for 2 h.

Figure 1 presents a schematic diagram showing the experimental setup used to measure the electrical response of the sensors [3]. A homemade arrangement for the sensor in the glass chamber was designed with a dynamic flow rate system to evaluate gas sensing performance. The target gas was injected into the chamber at the desired concentrations with a design including a mass controller arrangement for controlling the flow rate (1, 10, 30, 50, 70, or 100 ppm NO_2) via a hole in the cover of the chamber. A simple circuit was utilized to understand signals coming from the head of the sensor, which is further showcased by resistance values; later on, collection of data for evaluation and processing was done with a PC. All resistance measurements were averaged from multiple measurements obtained using a Jiehan5000 data acquisition system with the input voltage from a power supply (Vs) set at 4.0 V. S = Rg/Ra—which is the ratio that is used for the calculation of the response from the sensor [31], where Ra indicates the resistance in the presence of air and Rg indicates the resistance in the presence of NO_2 gas in the provided system. The times required for a 90% variation in resistance upon exposure to NO_2 or air are described as the response and recovery times. Selectivity toward NO_2 was assessed by exposing the sensor individually, including carbon monoxide, nitric oxide, methane (concentrations equal to 100 ppm), and further recording the characteristics of the response with corresponding values. Long-term stability was assessed by repeating the sensing measurements on multiple consecutive days.

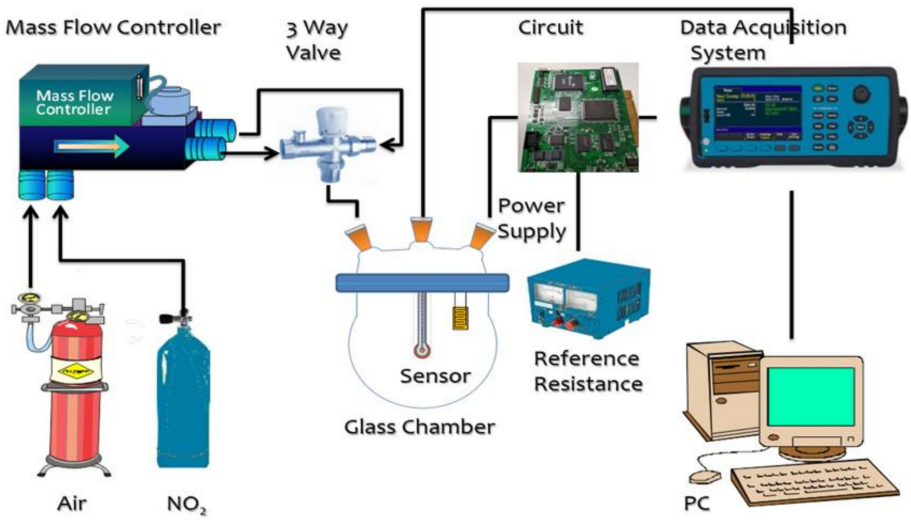

Figure 1. Diagrammatic representation of the experimental setup.

3. Results and Discussion

3.1. Structure Property

Figure 2 shows XRD measurements, indicating the phases and structure of pure $BivO_4$ and various $Pt/BiVO_4$ nanocomposites. The samples exhibited characteristic peaks corresponding to a structure of $BiVO_4$ (JCPDS 14-0688) with a monoclinic arrangement, as follows: 18.6° (110), 19.0° (011), 29.3° (121), 30.5° (040), 34.5° (200), 35.2° (002), 39.5° (211), 43.2° (051), 46.0° (042), 47.6° (240), 50.3° (202), 53.6° (161), 57.9° (321), and 59.3° (132) [19]. Peaks at 39.8° (111) and 46.0° (200) correspond to face-centred cubic Pt (JCPDS card: No. 04-0802) [32]. No other impurity peak was detected, indicating that the prepared samples were of high purity. Moreover, with increases in the amounts of deposited Pt, the diffraction peaks of Pt (111) were gradually intensified. Using Scherrer's equation, the mean Pt (111), $BiVO_4$ (051) and (161) crystalline sizes were estimated and listed in Table 1. Table 1 reveals that the crystalline sizes of Pt wt.% loading at 0.5%, 1%, 3%, 5% and 10% were 10.1 nm, 10.6 nm, 12.1 nm, 12.9 nm and 16.3 nm, respectively. The $BiVO_4$ (051) and (161) crystalline sizes were 24.2–25.8 nm and 25.8–28.2 nm, respectively. This shows that the Pt (111) crystalline size was increased by enlarging the amount of Pt loading. However, the $BiVO_4$ crystal size did not change greatly with the addition of platinum. These results indicate that the sensing material was a simple mixture.

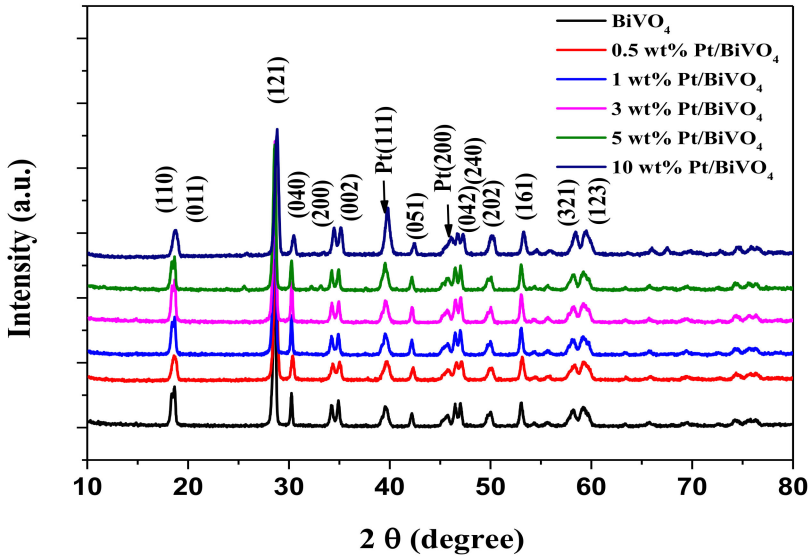

Figure 2. XRD patterns of different contents for $Pt/BiVO_4$ nanocomposites.

The morphology and microstructure of the $BiVO_4$ and $Pt/BiVO_4$ were characterized by FESEM and TEM evaluation of the nanocomposite structures. As shown in Figure 3a, SEM images revealed an arrangement comprising a large number of irregularly stacked $BiVO_4$ structures with an average diameter of 0.7–2.5 µm. Figure 3b shows the $Pt/BiVO_4$ nanocomposite containing Pt particles, with uneven diameters on the $BiVO_4$ sample. As shown in Figure 3c, TEM micrographs revealed d-spacing in the prescribed range of 0.227 and 0.196 nm, respectively corresponding to the original Pt-based (111) and (200) lattice plane [32]. As shown in Figure 3d, the EDS spectra confirmed the presence of Pt, V, Bi, Cu and O. The presence of strong signals from Cu can be ascribed to the Cu grid. Taken together, these confirm the formation of fully developed nanocomposites with a pure phase structure.

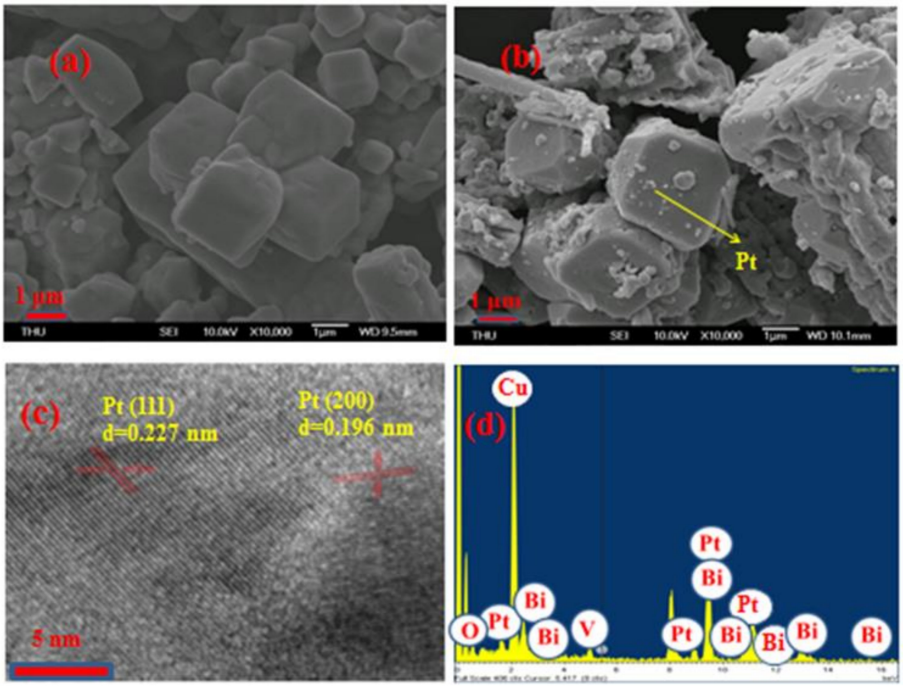

Figure 3. (**a**) FESEM images of $BiVO_4$ (**b**) Pt/$BiVO_4$; (**c**) TEM images of Pt/$BiVO_4$ (**d**) EDS spectrum of 3wt.% Pt/$BiVO_4$ nanocomposites.

3.2. Gas-Sensing Performance of Pt/BiVO$_4$

Figure 4a illustrates fluctuations in the response of sensors comprising (0, 0.5, 1, 3, 5 and 10) wt.% Pt/$BiVO_4$ nanocomposites following exposure to NO_2 gas at concentrations of 1–100 ppm at 25 °C. The increased response at all gas concentrations is indicative of typical n-type semiconductor behavior. The unloaded $BiVO_4$ materials exhibited a strong response (91.3) when exposed to high concentrations of NO_2 gas (100 ppm). Loading samples with a high concentration of Pt (10 wt.% Pt) increased the response strength substantially to 181.4. Table 1 lists the response times, recovery times, sensor responses, and base linearity results. The response and recovery times of sensors based on Pt/$BiVO_4$ nanocomposites were shorter than those of Pt/$BiVO_4$ nanocomposites. The 3 wt.% Pt/$BiVO_4$ nanocomposites achieved a T_{90} of only 12 s and a Tr_{90} of 35 s. As shown in Figure 4b, this sample also presented the highest linearity (R^2 = 0.992) and sensor response (S = 167.7).

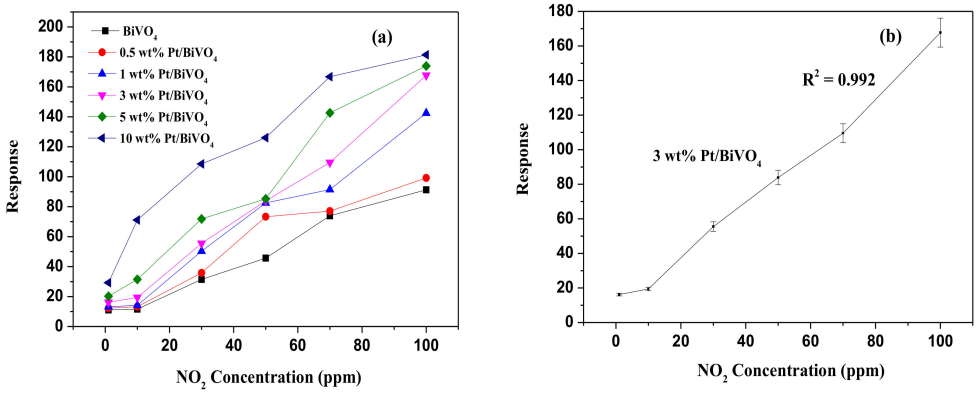

Figure 4. (**a**) Discrepancies in response relative to variations in 1–100 ppm NO_2 for varying Pt/$BiVO_4$ nanocomposites contents. (**b**) Response of the 3wt.% Pt/$BiVO_4$ sensor to 1–100 ppm NO_2 at room temperature.

Note that the response and recovery times of samples with high Pt concentrations (5 wt.% and 10 wt.%) were slower than those of the 3 wt.% Pt/$BiVO_4$ nanocomposite. These results are

similar to those reported in [31,33], indicating that at higher Pt concentrations, the formation of Pt aggregates tends to hinder the response and recovery of Pt/$BiVO_4$ nanocomposites. Overall, the 3 wt.% Pt/$BiVO_4$ sensor presented the best NO_2 sensing performance and was therefore selected as the gas sensor material for all subsequent experiments.

Response and recovery times are important parameters in sensor characterization and should be as short as possible. Figure 5a presents typical dynamic response curves as a function of the weight ratios of Pt/$BiVO_4$ when exposed to NO_2 at a concentration of 100 ppm at room temperature. Figure 5b presents the dynamic sensing curve of the Pt/$BiVO_4$ sensor when exposed to NO_2 gas at various concentrations (1–100 ppm). Table 1 lists sensing properties, sensor response times, recovery times, and linearity (R^2). The dramatic response of the sensors upon exposure to NO_2 is typical of n-type semiconductors.

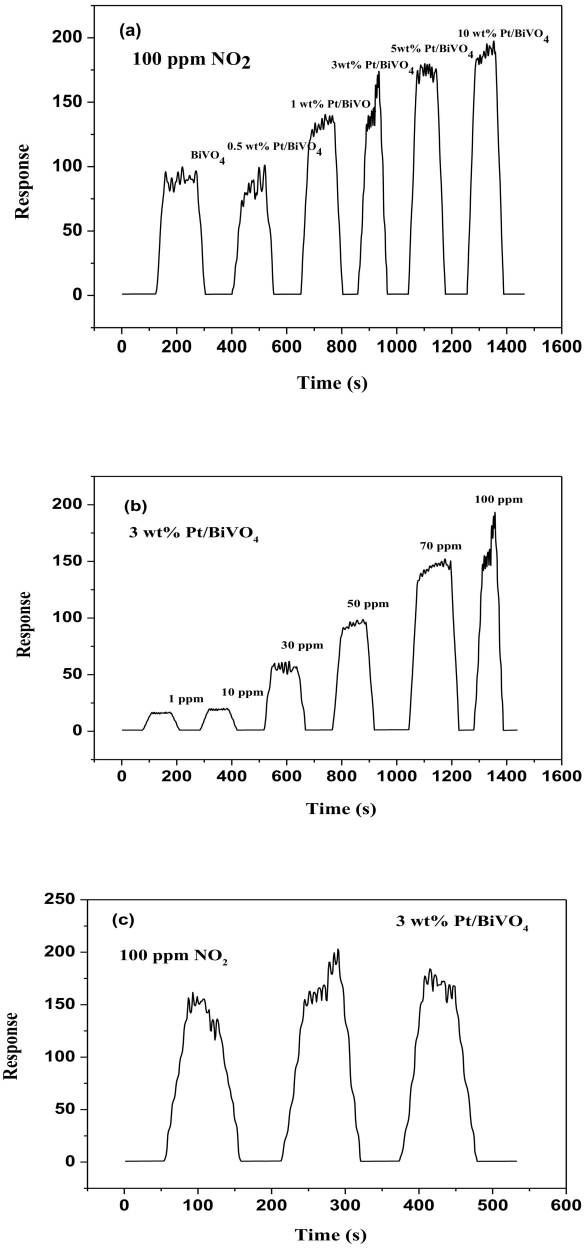

Figure 5. (**a**) The response for varying Pt/$BiVO_4$ nanocomposites contents of 100 ppm nitrogen dioxide at room temperature; (**b**) Curves for responses of the 3wt.% Pt/$BiVO_4$ in the range of 1–100 ppm nitrogen dioxide at room temperature; (**c**) Three-cycle repeated response curves of the 3wt.% Pt/$BiVO_4$ to 100 ppm nitrogen dioxide at room temperature.

We can see in Figure 5a that the strength of the responses increased with low NO_2 concentrations (1–100 ppm), as shown in Figure 5b. As shown in Figure 5c, the results from the proposed sensor maintained high reproducibility throughout the test cycle, thereby demonstrating that the Pt/$BiVO_4$ sensor could reliably be at this particular concentration level to monitor the concentration of NO_2.

Gas sensors are utilized and mostly evaluated with a range of selectivity, which is an important parameter. Figure 6 illustrates the responses of 3 wt.% Pt/$BiVO_4$ nanocomposites to NO_2, CO, NO, and CH_4 (100 ppm) at room temperature. Under these conditions, the response to NO_2 was 167.7, whereas the responses provided by the other selected gases were all lower, at a value of 30—thereby confirming the extraordinary selectivity demonstrated in 3 wt.% Pt/$BiVO_4$ nanocomposites to NO_2.

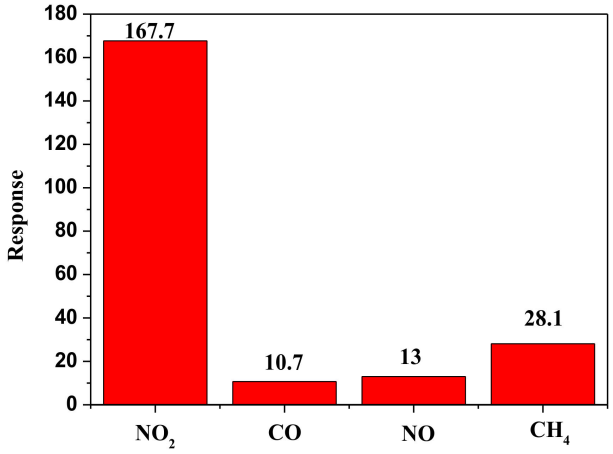

Figure 6. Selectivity test of the 3wt.% Pt/$BiVO_4$ nanocomposites to 100 ppm of various gases at room temperature.

As shown in Figure 7, we did not observe a significant decrease in the response of the 3 wt.% Pt/$BiVO_4$ nanocomposite despite continuous exposure to NO_2 (10 ppm) for a period of 10 days, thereby demonstrating the stability of the sensors.

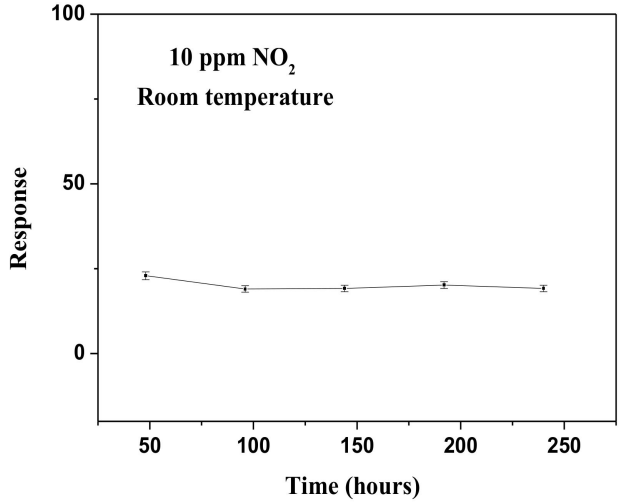

Figure 7. Stability of 3 wt.% Pt/$BiVO_4$ nanocomposites to 10 ppm NO_2 operating at room temperature.

3.3. Underlying Sensing Mechanism

This study demonstrated that the addition of Pb to $BiVO_4$ notably enhanced the response characteristics of the sensors. We assume that these effects are described by the provided reaction mechanism (1)–(4) [9,26,31,34,35]:

$$O_2(gas) + e^- \rightarrow O_2^-(ads) \quad (1)$$

$$NO_2(gas) \rightarrow NO_2(ads) \quad (2)$$

$$NO_2(ads) + O^-(ads) \rightarrow NO(gas) + O_2^-(ads) \quad (3)$$

$$NO_2(gas) + O_2^-(ads) + 2e^- \rightarrow NO_2^-(gas) + 2O^-(ads) \quad (4)$$

The enhancement mechanism was projected and illustrated in Figure 8. The Pt-based $BiVO_4$ nanocomposite exhibited typical n-type semiconductor behaviour [9,36]. When exposed to air, the active sites on the $BiVO_4$ started adsorbing the oxygen molecules, which in turn gave free electrons from the $BiVO_4$ material for the process of chemisorbed behaviour of oxygen ions (O_2^-) at RT (Equation (1)). The subsequent adsorption of NO_2 molecules at available adsorption sites on the BVO_4 surface enables the direct extraction of the surface electrons of the prepared sensor, producing a breaking of bond in the form of NO—the result of which leaves free oxygen ions (O_2^-) (Equations (2) and (3)) [37]. Catalysis of platinum can help in the enhancement of responsiveness of materials used for sensors to the various provided gases, due to a phenomenon referred to as the spillover effect [38,39]. The activity of Pt in this catalysis can help in accelerating the adsorption behaviour of molecular level oxygen; the adding of Pt dopants has a significant effect on surface area, which can lead to further chemisorbed oxygen species spillover, which increases the number of active sites on the $BiVO_4$ [11,26,33,40]. This increases the number of electrons that are captured, and in so doing enhances the response of the sensor. As shown in Equation (4), the availability of additional oxygen molecules for reactions with incoming NO_2 gas molecules increases the number of interactions between gas molecules in nitrous oxide and the sensing layer. The surface modification of $BiVO_4$ with platinum also increases the number of dissociated NO_2 molecules migrating to the surface of $BiVO_4$, thereby increasing responsivity to NO_2 gas. For comparison, the various NO_2 sensors based on Pt or $BiVO_4$ are listed in Table 2.

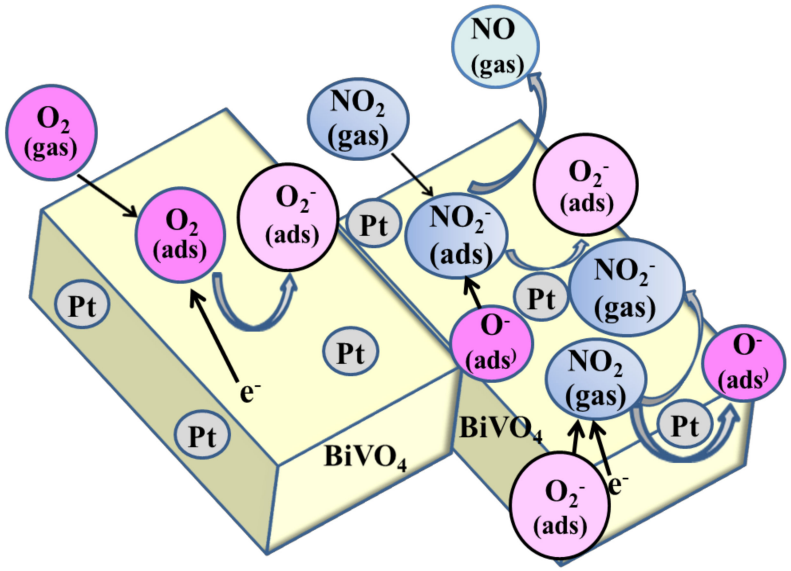

Figure 8. Schematic diagram of NO_2 gas sensing mechanism for Pt/$BiVO_4$ nanocomposite.

Table 2. Comparison of working temperature and various NO_2 sensors based on Pt or $BiVO_4$ nanocomposites.

Sensing Material	Response (Rg/Ra or Ra/Rg)	NO_2 (ppm)	Temperature (°C)	References
Pt-SnO_2	1.3	30	50	[41]
α-Fe_2O_3/$BiVO_4$	7.8	2	110	[10]
$BiVO_4$/Cu_2O	4.2	4	60	[34]
$BiVO_4$/Cu_2O/rGO	8.1	1	60	[9]
rGO-NiO-$BiVO_4$	8.1	2	60	[7]
Pt/WO_3	11.24	1	150	[35]
Pt/$BiVO_4$	167.7	100	25	This work

4. Conclusions

In this study, a Pt/$BiVO_4$ nanocomposite was prepared using a hydrothermal method with various weight percentages of platinum for use in NO_2 gas sensors. The structure and morphology of samples were characterized by XRD, TEM, FESEM, and EDX. The experiment results demonstrated that the addition of Pt to $BiVO_4$ at a concentration of 3 wt.% can greatly enhance the responsivity of Pt/$BiVO_4$ nanocomposite sensors to NO_2 at relatively low concentrations (100 ppm) as follows: sensor response (167.7), response time (12 s), and recovery time (35 s). The proposed Pt/$BiVO_4$ nanocomposite-based gas sensor exhibited promising nitrogen dioxide gas-sensing characteristics, including high sensitivity, high selectivity, and extremely short response/recovery times.

Author Contributions: Conceptualization, W.-D.L. and S.-Y.L.; methodology, W.-D.L.; software, W.-D.L.; validation, W.-D.L.; formal analysis, W.-D.L.; investigation, W.-D.L.; resources, W.-D.L.; data curation, W.-D.L. and S.-Y.L.; writing—original draft preparation, W.-D.L.; writing—review and editing, W.-D.L. and M.C.; visualization, W.-D.L. and S.-Y.L.; supervision, W.-D.L. and M.C. All authors have read and agreed to the published version of the manuscript.

Funding: This research received no external funding.

Institutional Review Board Statement: Not applicable.

Informed Consent Statement: Not applicable.

Data Availability Statement: The data presented in this study are available on request from the corresponding author. The data are not publicly available due to a complicated structure that requires additional explanations.

Acknowledgments: The authors are pleased for the help and support provided by Providence University, Taiwan and its Applied Chemistry section, in fabricating sensor humidity control.

Conflicts of Interest: The authors declare no conflict of interest.

References

1. Lim, S.H.; Feng, L.; Kemling, J.W.; Musto, C.J.; Suslick, K.S. An optoelectronic nose for the detection of toxic gases. *Nat. Chem.* **2009**, *1*, 562–567. [CrossRef]
2. Kampa, M.; Castanas, E. Human health effects of air pollution. *Environ. Pollut.* **2008**, *151*, 362–367. [CrossRef]
3. Zhu, Z.; Lin, S.-J.; Wu, C.-H.; Wu, R.-J. Synthesis of TiO_2 nanowires for rapid NO_2 detection. *Sens. Actuator A Phys.* **2018**, *272*, 288–294. [CrossRef]
4. Zhang, W.; Hu, M.; Liu, X.; Wei, Y.; Li, N.; Qin, Y. Synthesis of the cactus-like silicon nanowires/tungsten oxide nanowires composite for room-temperature NO_2 gas sensor. *J. Alloys Compd.* **2016**, *679*, 391–399. [CrossRef]
5. Liu, Y.; Gao, X.; Li, F.; Lu, G.; Zhang, T.; Barsan, N. Pt-In_2O_3 mesoporous nanofibers with enhanced gas-sensing performance towards ppb-level NO_2 at room temperature. *Sens. Actuator B Chem.* **2018**, *260*, 927–936. [CrossRef]
6. Sharma, B.; Sharma, A.; Myung, J.-h. Selective ppb-level NO_2 gas sensor based on SnO_2-boron nitride nanotubes. *Sens. Actuator B Chem.* **2021**, *331*, 129464. [CrossRef]
7. Bai, S.; Zhang, K.; Zhao, Y.; Li, Q.; Luo, R.; Li, D.; Chen, A. rGO decorated NiO-$BiVO_4$ heterojunction for detection of NO_2 at low temperature. *Sens. Actuator B Chem.* **2021**, *329*, 128912. [CrossRef]

8. Choi, S.W.; Katoch, A.; Sun, G.J.; Kim, S.S. Bimetallic Pd/Pt nanoparticle-functionalized SnO_2 nanowires for fast response and recovery to NO_2. *Sens. Actuator B Chem.* **2013**, *181*, 446–453. [CrossRef]
9. Li, Q.; Han, N.; Zhang, K.; Bai, S.; Guo, J.; Luo, R.; Li, D.; Chen, A. Novel p-n heterojunction of $BiVO_4/Cu_2O$ decorated with rGO for low concentration of NO_2 detection. *Sens. Actuator B Chem.* **2020**, *320*, 128284. [CrossRef]
10. Bai, S.; Tian, K.; Fu, H.; Feng, Y.; Luo, R.; Li, D.; Chen, A.; Liu, C.C. Novel α-$Fe_2O_3/BiVO_4$ heterojunctions for enhancing NO_2 sensing properties. *Sens. Actuator B Chem.* **2018**, *268*, 136–143. [CrossRef]
11. Zhu, Z.; Lin, Y.-C.; Chung, C.-L.; Wu, R.-J.; Huang, C.-L. A novel composite of triangular silver nanoplates on $BiVO_4$ for gaseous formaldehyde degradation. *Appl. Surf. Sci.* **2021**, *543*, 148784. [CrossRef]
12. Yang, J.; Shi, Q.; Zhang, R.; Xie, M.; Jiang, X.; Wang, F.; Cheng, X.; Han, W. $BiVO_4$ quantum tubes loaded on reduced graphene oxide aerogel as an efficient photocatalyst for gaseous formaldehyde degradation. *Carbon* **2018**, *138*, 118–124. [CrossRef]
13. Qiao, X.; Xu, Y.; Yang, K.; Ma, J.; Li, C.; Wang, H.; Jia, L. Mo doped $BiVO_4$ gas sensor with high sensitivity and selectivity towards H_2S. *Chem. Eng. J.* **2020**, *395*, 125144. [CrossRef]
14. Li, C.; Qiao, X.; Jian, J.; Feng, F.; Wang, H.; Jia, L. Ordered porous $BiVO_4$ based gas sensors with high selectivity and fast-response towards H_2S. *Chem. Eng. J.* **2019**, *375*, 121924. [CrossRef]
15. Li, F.; Leung, D.Y.C. Highly enhanced performance of heterojunction $Bi_2S_3/BiVO_4$ photoanode for photoelectrocatalytic hydrogen production under solar light irradiation. *Chem. Eng. Sci.* **2020**, *211*, 115266. [CrossRef]
16. Li, F.; Zhao, W.; Leung, D.Y.C. Enhanced photoelectrocatalytic hydrogen production via Bi/$BiVO_4$ photoanode under visible light irradiation. *Appl. Catal. B Environ.* **2019**, *258*, 117954. [CrossRef]
17. Chen, L.; Zhang, M.; Yang, J.; Li, Y.; Sivalingam, Y.; Shi, Q.; Xie, M.; Han, W. Synthesis of $BiVO_4$ quantum dots/reduced graphene oxide composites for CO_2 reduction. *Mater. Sci. Semicond. Process.* **2019**, *102*, 104578. [CrossRef]
18. Li, X.; Wei, D.; Ye, L.; Li, Z. Fabrication of Cu_2O-RGO/$BiVO_4$ nanocomposite for simultaneous photocatalytic CO_2 reduction and benzyl alcohol oxidation under visible light. *Inorg. Chem. Commun.* **2019**, *104*, 171–177. [CrossRef]
19. Talasila, G.; Sachdev, S.; Srivastava, U.; Saxena, D.; Ramakumar, S.S.V. Modified synthesis of $BiVO_4$ and effect of doping (Mo or W) on its photoelectrochemical performance for water splitting. *Energy Rep.* **2020**, *6*, 1963–1972. [CrossRef]
20. Luo, J.; Fu, P.; Qu, Y.; Lin, Z.; Zeng, W. The n-butanol gas-sensing properties of monoclinic scheelite $BiVO_4$ nanoplates. *Phys. E* **2018**, *103*, 71–75. [CrossRef]
21. Lin, Y.; Cai, H.; Chen, H.; Luo, H. One–pot synthesis of $Bi_4V_2O_{11}/BiVO_4$ heterostructure with enhanced photocatalytic activity for dye degradation. *Appl. Surf. Sci.* **2021**, *544*, 148921. [CrossRef]
22. Malathi, A.; Madhavan, J.; Ashokkumar, M.; Prabhakarn, A. A review on $BiVO_4$ photocatalyst: Activity enhancement methods for solar photocatalytic applications. *Appl. Catal.* **2018**, *555*, 47–74.
23. Abdi, F.F.; Savenije, T.J.; May, M.M.; Dam, B.; van de Krol, R. The origin of slow carrier transport in $BiVO_4$ thin film photoanodes: A time-resolved microwave conductivity study. *J. Phys. Chem. Lett.* **2013**, *4*, 2752–2757. [CrossRef]
24. Zhou, B.; Zhao, X.; Liu, H.; Qu, J.; Huang, C.P. Visible-light sensitive cobalt-doped $BiVO_4$ (Co-$BiVO_4$) photocatalytic composites for the degradation of methylene blue dye in dilute aqueous solutions. *Appl. Catal. B Environ.* **2010**, *99*, 214–221. [CrossRef]
25. Wang, M.; Guo, P.; Chai, T.; Xie, Y.; Han, J.; You, M.; Wang, Y.; Zhu, T. Effects of Cu dopants on the structures and photocatalytic performance of cocoon-like Cu-$BiVO_4$ prepared via ethylene glycol solvothermal method. *J. Alloys Compd.* **2017**, *691*, 8–14. [CrossRef]
26. Mohamed, R.M.; Mkhalid, I.A.; Shawky, A. Facile synthesis of Pt–$In_2O_3/BiVO_4$ nanospheres with improved visible-light photocatalytic activity. *J. Alloys Compd.* **2019**, *775*, 542–548. [CrossRef]
27. Cao, S.-W.; Yin, Z.; Barber, J.; Boey, F.Y.C.; Loo, S.C.J.; Xue, C. Preparation of Au-$BiVO_4$ Heterogeneous Nanostructures as Highly Efficient Visible-Light Photocatalysts. *ACS Appl. Mater. Interfaces* **2012**, *4*, 418–423. [CrossRef] [PubMed]
28. Wang, M.; Han, J.; Lv, C.; Zhang, Y.; You, M.; Liu, T.; Li, S.; Zhu, T. Ag, B, and Eu tri-modified $BiVO_4$ photocatalysts with enhanced photocatalytic performance under visible-light irradiation. *J. Alloys Compd.* **2018**, *753*, 465–474. [CrossRef]
29. Wang, W.; Wang, J.; Wang, Z.; Wei, X.; Liu, L.; Ren, Q.; Gao, W.; Liang, Y.; Shi, H. p–n junction CuO/$BiVO_4$ heterogeneous nanostructures: Synthesis and highly efficient visible-light photocatalytic performance. *Dalton Trans.* **2014**, *43*, 6735–6743. [CrossRef] [PubMed]
30. Fujimoto, I.; Wang, N.; Saito, R.; Miseki, Y.; Gunji, T.; Sayama, K. $WO_3/BiVO_4$ composite photoelectrode prepared by the improved auto-combustion method for highly efficient water splitting. *Int. J. Hydrogen Energy* **2014**, *39*, 2454–2461. [CrossRef]
31. Samerjai, T.; Tamaekong, N.; Liewhiran, C.; Wisitsoraat, A.; Phanichphant, S. NO_2 gas sensing of flame-made Pt-loaded WO_3 thick films. *J. Solid State Chem.* **2014**, *214*, 47–52. [CrossRef]
32. Mirzaei, A.; Bang, J.H.; Choi, M.S.; Han, S.; Lee, H.Y.; Kim, S.S.; Kim, H.W. Changes in characteristics of Pt-functionalized RGO nanocomposites by electron beam irradiation for room temperature NO_2 sensing. *Ceram. Int.* **2020**, *46*, 21638–21646. [CrossRef]
33. Wang, C.-Y.; Hong, Z.-S.; Wu, R.-J. Promotion effect of Pt on a SnO_2–WO_3 material for NOx sensing. *Phys. E* **2015**, *69*, 191–197. [CrossRef]
34. Bai, S.; Li, Q.; Han, N.; Zhang, K.; Tang, P.; Feng, Y.; Luo, R.; Li, D.; Chen, A. Synthesis of novel $BiVO_4/Cu_2O$ heterojunctions for improving $BiVO_4$ towards NO_2 sensing properties. *J. Colloid Interface Sci.* **2020**, *567*, 37–44. [CrossRef]
35. Liu, H.; Xu, Y.; Zhang, X.; Zhao, W.; Ming, A.; Wei, F. Enhanced NO_2 sensing properties of Pt/WO_3 films grown by glancing angle deposition. *Ceram. Int.* **2020**, *46*, 21388–21394. [CrossRef]

36. He, H.; Zhou, Y.; Ke, G.; Zhong, X.; Yang, M.; Bian, L.; Lv, K.; Dong, F. Improved Surface Charge Transfer in MoO_3/$BiVO_4$ Heterojunction Film for Photoelectrochemical Water Oxidation. *Electrochim. Acta* **2017**, *257*, 181–191. [CrossRef]
37. Zhang, C.; Luo, Y.; Xu, J.; Debliquy, M. Room temperature conductive type metal oxide semiconductor gas sensors for NO_2 detection. *Sens. Actuators A Phys.* **2019**, *289*, 118–133. [CrossRef]
38. Cabot, A.; Arbiol, J.; Morante, J.R.; Weimar, U.; Bârsan, N.; Göpel, W. Analysis of the noble metal catalytic additives introduced by impregnation of as obtained SnO_2 sol-gel nanocrystals for gas sensors. *Sens. Actuator B Chem.* **2000**, *70*, 87–100. [CrossRef]
39. Bang, J.H.; Mirzaei, A.; Han, S.; Lee, H.Y.; Shin, K.Y.; Kim, S.S.; Kim, H.W. Realization of low-temperature and selective NO_2 sensing of SnO_2 nanowires via synergistic effects of Pt decoration and Bi_2O_3 branching. *Ceram. Int.* **2021**, *47*, 5099–5111. [CrossRef]
40. Lu, Y.; Jing, H.; Yu, H.; Zhao, Y.; Li, Y.; Huo, M. Enhanced catalytic performance of $BiVO_4$/Pt under the combination of visible-light illumination and ultrasound waves. *J. Taiwan Inst. Chem. E* **2019**, *102*, 133–142. [CrossRef]
41. Zhang, Q.; Wang, T.; Sun, Z.; Xi, L.; Xu, L. Performance improvement of photoelectrochemical NO_2 gas sensing at room temperature by $BiVO_4$-polyoxometalate nanocomposite photoanode. *Sens. Actuator B Chem.* **2018**, *272*, 289–295. [CrossRef]